RESEARCH ARTICLE

National Science Open
5: 20250084, 2026
https://doi.org/10.1360/nso/20250084

Materials Science

Special Topic: Hollow Multishelled Structure

Photothermal activation by hollow multishelled structure for efficient uranium extraction

Sania Shabbir[1,2,#], Dan Yu[1,2,#], Shuhui Zhan[1,2], Jiangtao Hu[3], Jiawei Wan[1,2], Guozhong Wu[3], Nailiang Yang[1,2,*] & Dan Wang[1,4,*]

[1]*State Key Laboratory of Biopharmaceutical Preparation and Delivery, Institute of Process Engineering, Chinese Academy of Sciences, Beijing 100190, China;*
[2]*University of Chinese Academy of Sciences, Beijing 100049, China;*
[3]*Shanghai Institute of Applied Physics, Chinese Academy of Sciences, Shanghai 201800, China;*
[4]*College of Chemistry and Environmental Engineering, Shenzhen University, Shenzhen 518060, China*

#Contributed equally to this work.
*Corresponding authors (emails: nlyang@ipe.ac.cn (Nailiang Yang); danwang@szu.edu.cn (Dan Wang))

Received 28 December 2025; Revised 26 February 2026; Accepted 16 March 2026; Published online 17 March 2026

Abstract: Uranium extraction from seawater is essential for sustainable nuclear energy but remains kinetically limited by ultralow concentration and slow ion diffusion. Inspired by the Stokes-Einstein equation, we can predict that the rise in local temperature would increase the diffusion coefficient for uranyl ions. Here we report a generalizable photothermal strategy by depositing amorphous Ta_2O_5/C-HoMS (hollow multishelled structure) onto amidoxime-functionalized polyethylene fibers. The unique multi-shelled and compartmentalized architecture of HoMS facilitates both efficient solar-to-thermal conversion and enhanced mass transport. Under solar irradiation, the composite generates localized heating, which accelerates uranyl diffusion and raises the adsorption capacity by 27% compared to dark conditions, while maintaining over 91% capacity after seven consecutive adsorption-desorption cycles. Systematic light-versus-dark comparisons demonstrate that the photothermal effect is the key driver for enhanced kinetics for uranium uptake. This work provides a simple, universal and efficient platform for solar-driven uranium recovery, paving a practical route toward sustainable nuclear fuel supply from the ocean.

Keywords: hollow multishelled structure, uranium extraction, photothermal conversion, Ta_2O_5/C

INTRODUCTION

Uranium is anticipated to become a primary fuel source by the mid−21st century as fossil fuels deplete, and nuclear power offers a clean, low−carbon energy alternative [1,2]. Since the launch of 'Project Oyster' in the 1950s, extracting uranium from seawater has been pursued as a potentially sustainable nuclear fuel supply [3–5]. The oceans contain an estimated 4.5 billion tons of uranium, primarily in the form of dissolved uranyl ions, whose reserves are about 1000 times larger than terrestrial resources [5–10]. Over the past decades, numerous adsorbents have been developed for this purpose, with amidoxime−based polymers showing particularly high affinity and selectivity toward uranium in marine environments [9,11,12]. However, the

practical implementation of uranium extraction from seawater remains constrained by several inherent challenges in marine environments because of the slow adsorption kinetics [13–16]. Traditional adsorbent modifications, such as optimizing pore structure, surface area, and ligand density, have partially mitigated these limitations. Consequently, there is a pressing need for a universal approach that utilizes external stimuli to actively enhance the adsorption process [17–20]. Heat, as a form of energy input, is particularly effective in accelerating reaction kinetics and promoting ion diffusion. Converting abundant solar energy into localized heat through photothermal materials offers a sustainable route to provide this thermal stimulus. Among various photothermal candidates, Ta_2O_5/C based hollow multishelled structures (HoMSs) stand out due to their excellent chemical stability in marine environments and efficient light-to-heat conversion capability [21,22]. The unique HoMS architecture offers excellent light absorption, efficient heat localization, and favorable mass-transfer properties, making them ideal candidate for coupling photothermal effects with uranium adsorption. Hollow multiple structures can significantly enhance the energy utilization and mass transport due to their unique properties. HoMS offers multiple internal reflected interfaces, which promotes repeated light scattering and increases the optical path length within the material. This effect significantly increases the absorption and conversion of solar energy. The hierarchical hollow cavities help to store thermal energy and prevent heat loss, which maintains the local temperature high and further promotes uranium adsorption. Meanwhile, the hierarchical hollow cavities with porous shells minimize the mass transfer pathways, offer a large number of easily accessible active sites and speed up the diffusion of reactants and products. As a result, by maintaining a localized thermal field and minimizing the heat loss, the interconnected empty spaces would improve reaction kinetics significantly. By integrating such light-responsive materials with amidoxime-functionalized fibers, it is possible to overcome the kinetic barrier without requiring external electrical energy or bulk heating [23–25]. In this work, we select the well-studied amidoxime-functionalized polyethylene fiber as the model substrate to explicitly reveal the influence of the photothermal effect on uranium extraction. By facilely depositing Ta_2O_5/C-HoMS onto these fibers, we fabricate a composite adsorbent. Under solar irradiation, the photothermal coating converts light into localized heat, which significantly enhances uranium adsorption kinetics and capacity (Scheme 1) [26–28]. Through systematic comparison between light and dark conditions, we demonstrate that this photothermal strategy can increase the temperature not only at the irradiated zone but also in the localized regions under water, thereby improving the uranium uptake, while exhibiting good stability and reusability. This study provides a practical, universal and energy-efficient pathway toward enhancing seawater uranium extraction, contributing to the sustainable supply of nuclear fuel in the future.

RESULTS AND DISCUSSION

The Ta_2O_5/C-HoMS were synthesized via a sequential templating approach, as reported previously [21]. Scanning electron microscopy (SEM) images reveal that the obtained HoMS particles exhibit a uniform spherical morphology with an average diameter of approximately 1.3 μm and a distinct wrinkled surface (Figure 1a and Figure S1). Further structural details are provided by transmission electron microscopy (TEM), which clearly shows the characteristic multishelled architecture with well-defined layers (Figure 1b). This unique hollow and multilayered configuration, combined with the surface texturing, contributes to a

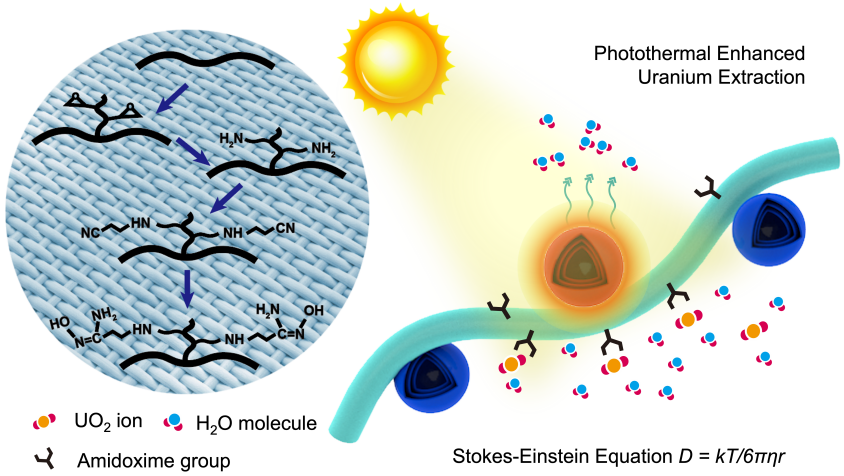

Scheme 1 Schematic illustration of the composite adsorbent design and its proposed photothermal adsorption mechanism. The amidoxime functionalization of the polyethylene fiber was achieved via radiation-induced grafting, creating selective binding sites for uranium. Under solar irradiation, the loaded Ta_2O_5/C hollow multishelled structure efficiently converts light into localized heat. This heating promotes water evaporation and elevates the interfacial temperature, which in turn accelerates the diffusion of uranyl ions toward the adsorbent surface according to the Stokes-Einstein equation. The combined effects of thermally enhanced diffusion and selective chelation by amidoxime groups lead to significantly improved uranium adsorption kinetics.

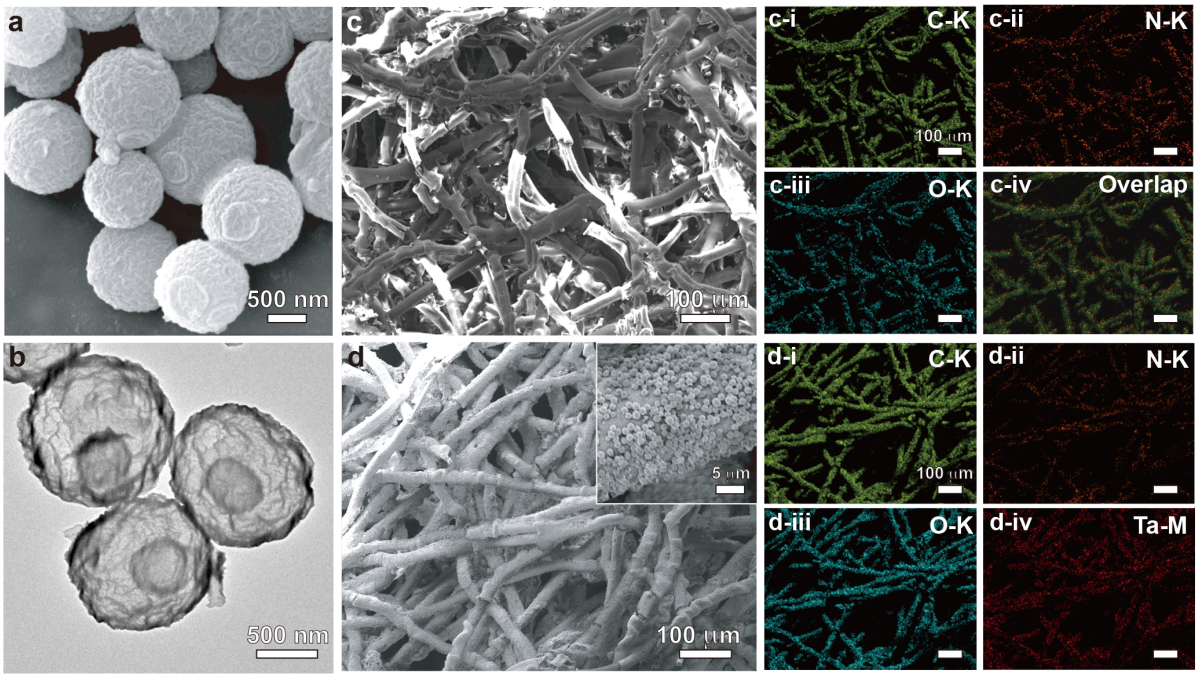

Figure 1 (a) SEM and (b) TEM images of Ta_2O_5/C-HoMS. SEM images of (c) fiber and (d) Fiber@HoMS. Inset of (d) is the enlargement of Fiber@HoMS. (i–iv) The corresponding EDS mapping images of (c) and (d).

high specific surface area and is expected to facilitate efficient light absorption and heat localization, which are the key attributes for enhancing photo-thermal conversion and subsequent uranium adsorption performance.

The pristine fiber is composed of carbon, nitrogen, and oxygen, has a smooth, uniform surface that is

consistent with its polymeric nature, according to SEM with energy-dispersive X-ray spectroscopy (SEM-EDX) (Figure 1c). The distribution of different elements within the fiber is shown in the relevant elemental mapping images (Figure 1c-i to c-iv). In particular, the green signals in (Figure 1c-i) indicate that carbon (C-K) is the predominant element in the fiber. The existence of the amidoxime functional groups, which are essential for uranium capture, is confirmed by nitrogen (N-K) mapping in Figure 1c-ii. The oxygen concentration is revealed by oxygen (O-K) mapping in (Figure 1c-iii), most likely from the amidoxime functional groups and any leftover groups on the fiber surface. The overlap image (Figure 1c-iv) verifies the functionalization of the fiber by displaying the combined presence of carbon, nitrogen, and oxygen. Moreover, the X-ray photoelectron spectroscopy (XPS) and Fourier transform infrared spectroscopy (FTIR) analyses collectively verify the successful fabrication of the amidoxime-functionalized fiber, as evidenced by the characteristic N–H (400.1 eV) and C=N (399.0 eV) species from the N 1s signal, and C=O (531.5 eV) and N–O–H (532.5 eV) species from the O 1s signal, along with the FTIR peaks at 3000–3500, 1650, and 930 cm^{-1} corresponding to the amidoxime groups (Figures S2 and S3). Following deposition with Ta_2O_5/C-HoMS, the fiber surface exhibits a markedly altered morphology characterized by increased roughness and a uniform coverage of granular particles, as shown in the SEM images (Figure 1d and inset). The originally smooth polymeric surface is transformed into a hierarchically structured interface. EDX elemental mapping shows a strong Ta signal, which is consistently detected across the coated region (Figure 1d-iv), accompanied by a correspondingly enhanced oxygen signal (Figure 1d-iii), while the underlying C and N signals from the fiber remain present (Figure 1d-i, d-ii). The continuous spatial distribution of Ta and O confirms the formation of a coherent and uniform Ta_2O_5/C-HoMS coating over the fiber surface.

The X-ray diffraction (XRD) pattern of the pristine polyethylene fiber presents the characteristic diffraction peaks observed in the 2θ range from 15° to 30° (Figure 2a), which corresponds to the ordered packing of polymer chains within the crystalline regions, confirming the well-defined crystalline structure of the base adsorbent material. In contrast, the XRD curve of Ta_2O_5/C-HoMS indicates the long-range disorder feature, which plays a significant role in heat localization and mass transfer enhancement [21] during subsequent uranium extraction. Notably, there is no distinguishable change in the diffraction curves after uranium adsorption. It indicates the HoMS loading with ethyl acetate and the uranium adsorption did not destroy the molecular chain of the fiber, showing the good stability of the fiber. Furthermore, there are no new sharp peaks in the post-adsorption pattern, indicating that no crystalline uranium or its oxide was formed, suggesting that uranium is adsorbed as a well-dispersed complex form on the fiber surface. The ultraviolet-visible near-infrared (UV-vis-NIR) spectrum shows that the Ta_2O_5/C-HoMS has a broad absorption in the visible light range, while the fiber had a better performance in the range over 1800 nm (Figure 2b). Notably, the Fiber@HoMS exhibits stronger and broader absorption over the entire solar spectrum than either the pristine Ta_2O_5/C-HoMS or the amidoxime-functionalized fiber. This enhanced and spectrally complementary absorption of the Fiber@HoMS directly translates to superior photothermal conversion. Under light irradiation, the dry composite rapidly reaches a surface temperature exceeding 90 °C. Even in a wetted state under seawater conditions, the composite maintains a stable localized temperature of over 40 °C, confirming efficient photothermal activity in increasing the localized temperature (Figure 2c). Side-view IR thermal imaging after 30 min of irradiation further shows a sustained vertical temperature gradient from the water surface downward, with the submerged fiber region remaining notably warmer than the ambient solution (Figure 2d, e). The elevated temperature and established thermal gradient are driven by conductive

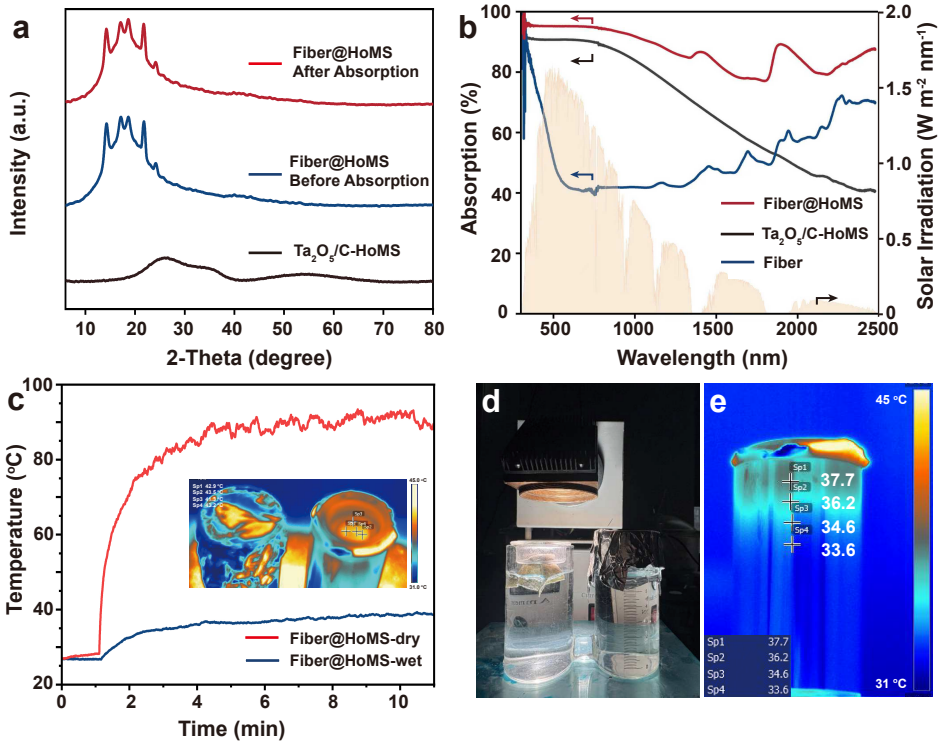

Figure 2 (a) XRD patterns of fiber before and after uranium adsorption and Ta_2O_5/C-HoMS. (b) UV-vis-NIR absorption and (c) photo-thermal performance for various samples. (d) Digital image of uranium absorption equipment under irradiation. (e) IR image of the aforementioned adsorption equipment with temperature gradient during irradiation on Fiber@HoMS for 30 min.

and convective heat transfer. This localized heat reduces the kinetic viscosity of water and, according to the Stokes-Einstein equation ($D = kT/6\pi\eta r$), enhances the diffusion coefficient of uranyl ions, thereby providing a driving force for accelerated adsorption [29,30]. Uranium adsorption was conducted by immersing 10 mg of composite adsorbent in uranium solution at a pH of 8.0, adjusted by Na_2CO_3. The Ta_2O_5/C-HoMS fiber was tested under simulated solar irradiation with an intensity of 1000 W/m^2 and all reported data are averaged from triplicate experiments. The adsorption kinetics of uranium was studied by establishing the time-dependent extraction profiles in a tank containing 25 L of solution (Figure S4). By comparing the Fiber@HoMS composite under irradiation or in the dark (Figure 3a), both systems exhibited rapid adsorption within the initial 10 h, achieving approximately 50% of the equilibrium capacity (Figure 3b). The adsorption rate subsequently slowed as equilibrium was approached. Notably, the Fiber@HoMS consistently showed higher uranium uptake under irradiation than its counterpart in the dark at each corresponding time point. These adsorption data were well matched with the Langmuir isotherm model with a R^2 over 0.99, indicating monolayer adsorption on a homogeneous surface [31–33]. The calculated maximum adsorption capacities were 412 mg/g for the photo-thermal system and 324 mg/g for the dark one, which align closely with the experimental values. The uptake increased with time until saturation was reached, demonstrating the effectiveness of the fiber for uranium adsorption. The slope of this plot at different stages provides insight into the rate constants and the underlying adsorption mechanism. Kinetic analysis further revealed that the adsorption process for both fibers follows a pseudo-second-order model, as evidenced by the linear plot of t/q_t versus time (Figure 3c). This suggests that chemisorption is the rate-determining step [34], and the higher

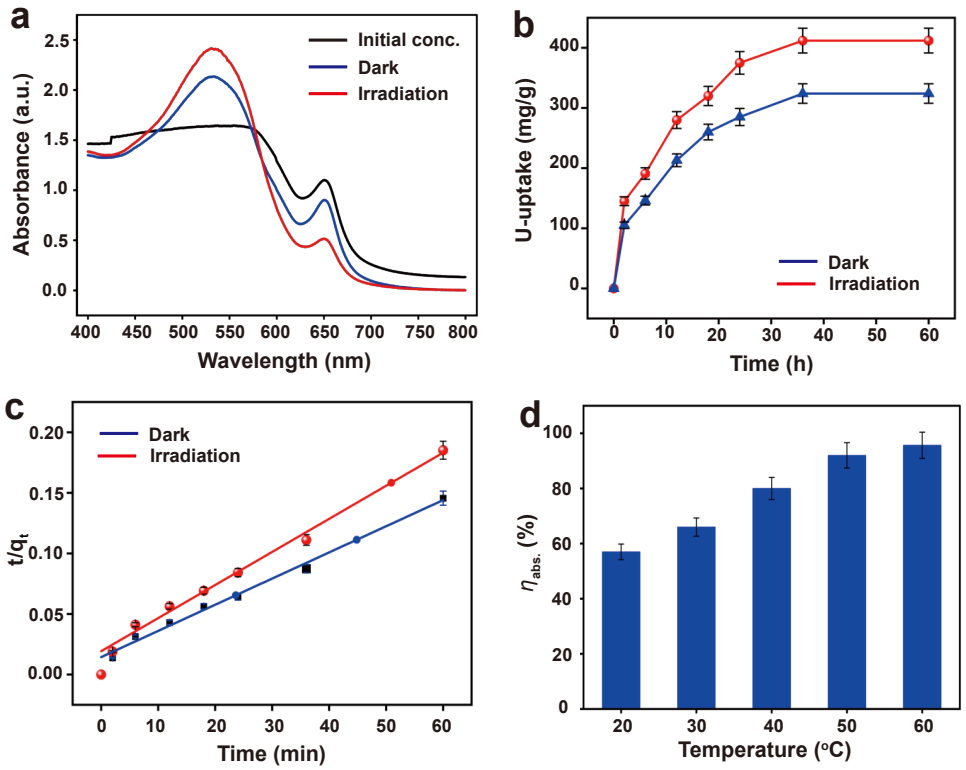

Figure 3 (a) UV-vis spectra in dark and irradiation after 1 h absorption. (b) Uranium uptake over time in dark and irradiation conditions. (c) Thermal effect on absorbance across the measured range. The ratios are calculated from the data after absorption for 6 h. (d) Dynamic adsorption behaviour of uranium adsorption.

temperature can promote the absorption kinetics.

To further investigate the influence of temperature on uranium adsorption, experiments were conducted at varying temperatures from 20 to 60 °C under steady conditions within a 250 mL uranium solution. It was found that the uranium adsorption capacity increased monotonically with increasing temperature in the first 6 h. Around 96% of uranium ions can be adsorbed in the solution around 60 °C, while it is only 58% when the temperature decreases to 20 °C (Figure 3d). This trend further proves that the elevated temperature promotes ion diffusion and accelerates the surface coordination, thereby improving both capacity and kinetics [35–37]. These results offer valuable implications for practical applications. On one hand, the positive temperature dependence supports the use of focused sunlight to create localized heating at the adsorption interface, which can further enhance uranium uptake kinetics without bulk solution heating. On the other hand, elevated local temperature can also help suppress microbial colonization on the material surface, mitigating biofouling and extending the operational lifetime of the adsorbent [38,39]. Future work can focus on quantitatively regulating the photo-thermal temperature rise, evaluating long-term cycling stability, and validating performance under realistic seawater conditions. To probe the spatial distribution of uranium uptake, the adsorbed fiber was analyzed by SEM-EDX at six defined locations (Figure 4a). These included: the center of the floating section above water (resting on the insulating pad); the air-water interface (meniscus region, where the fiber enters the water, termed the edge); and submerged points at 1, 2, 3, and 4 cm below the surface. The uranium content is reported as the weight percentage (wt%) of U within the analyzed fiber segment (Figure 4b). In the dark, negligible uranium was detected in the center (above-water) section. At the air-water

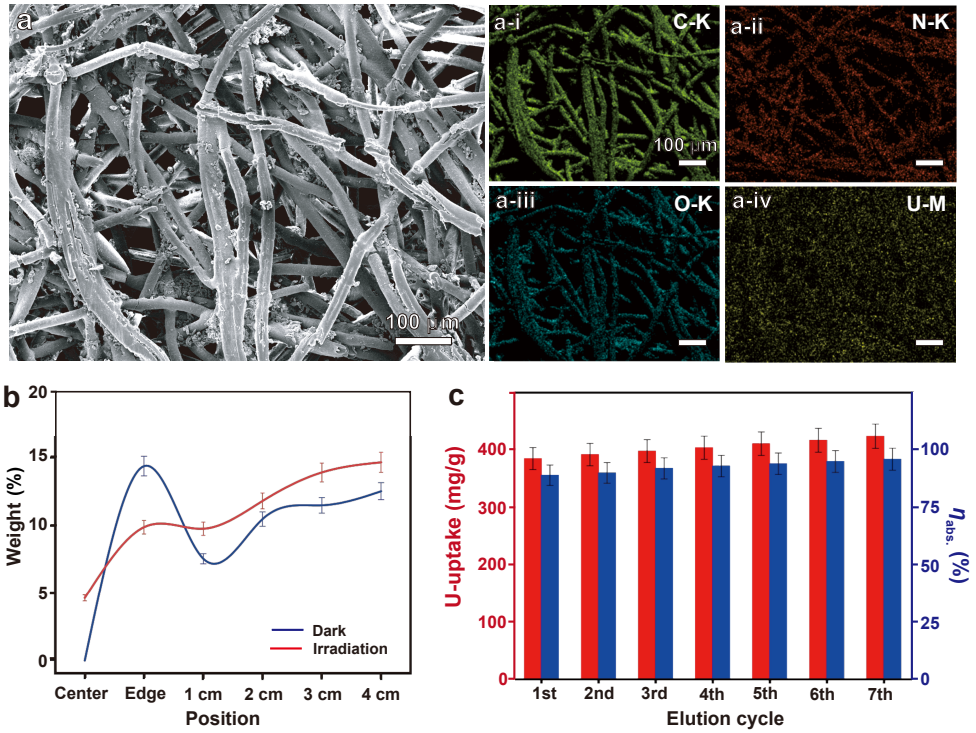

Figure 4 (a) SEM-EDX analysis of Fiber@HoMS after absorption. (b) Uranium adsorption (wt%) at various positions and depths. (c) Uranium adsorption recycle performance over successive elution.

interface (edge), however, the uranium content reached 14.41 wt%, which is attributed to localized concentration enrichment driven by faster evaporation at the meniscus. Under light irradiation, the spatial adsorption profile changed distinctly. A measurable uranium uptake (5.69 wt%) occurred even on the above-water center section, indicating vapor-phase transport of hydrated uranyl ions activated by photo-thermal evaporation. Interestingly, at the air-water interface, the uranium content (7.39 wt%) was lower than that in the dark. This apparent reduction can be explained by a competition and interception effect that the photo-thermal process not only intensifies evaporation at the edge but, more significantly, enhances uranium adsorption in the submerged zone. As presented in Figure 2e, heat exchange and conduction occur between Ta_2O_5/C-HoMS, fibers and water. Consequently, the water below the insulation pad was also heated under irradiation, leading to enhanced adsorption capacity. The weight ratios reached 10.38%–15.34 wt%, uniformly exceeding those of 8.86%–12.48% in the dark. This improvement is governed by temperature-activated ion transport. According to the Stokes-Einstein equation, the rise in local temperature (T) increases the diffusion coefficient (D) of uranyl ions. The photo-thermally generated heat along the fiber thus accelerates mass transfer, mitigates diffusion-limited kinetics at depth, and replenishes the uranium supply at the adsorption interface more rapidly. Meanwhile, the Fiber@HoMS also shows good reusability through seven consecutive adsorption-desorption cycles with 1.0 mol/L Na_2CO_3 as the eluent (Figure 4c). Desorption proceeded efficiently via the formation of soluble uranyl-carbonate complexes, achieving near-complete uranium recovery in each cycle. The adsorbent exhibited excellent regeneration stability, retaining over 91% of its initial adsorption capacity after the seventh cycle, which underscores its robust chemical stability and practical reusability.

CONCLUSIONS

This study demonstrates a photo-thermal strategy for enhancing uranium extraction from seawater, based on the integration of Ta_2O_5/C hollow multishelled structures onto amidoxime-functionalized polyethylene fibers. Under light irradiation, the Ta_2O_5/C-HoMS coating efficiently converts solar energy into localized heat, which accelerates ion diffusion and thereby significantly improves uranium adsorption kinetics, compared to a control experiment under dark conditions. The composite adsorbent exhibits a facile and robust fabrication route along with excellent reusability across multiple adsorption-desorption cycles. It can be predicted that combining this photo-thermal adsorption system with renewable energy-driven marine platforms or integrating it with desalination processes will offer a synergistic approach to resource recovery and freshwater production. It also provides a promising pathway toward sustainable, energy-efficient uranium recovery from the ocean, supporting the future supply of nuclear fuel.

MATERIALS AND METHODS

Materials

Fibers for the uranium extraction were fabricated by a radiation grafting approach [40]. Ta_2O_5/C-HoMS was fabricated by the reported sequential templating approach [21,22]. Uranyl nitrate hexahydrate $UO_2(NO_3)_2 \cdot 6H_2O$ (99%), Arsenazo III $C_{22}H_{18}(As_2)\ N_4O_{14}S_2$ (99%) were purchased from Shanghai Aladdin Biochemical Technology Co., Ltd. All the reagents were used without further purification.

Methods

Preparation of Ta_2O_5/C-HoMS via sequential templating approach

Carbon microspheres (CMSs) were synthesized by hydrothermal polymerization of sucrose, which were initially prepared as a sacrificial template. Then the $TaCl_5$ was gradually adsorbed and subjected to regular heat treatment as a part of the sequential templating technique to prepare the HoMS samples. These CMSs (0.6 g) were then added to a 30 mL solution of $TaCl_5$ (0.1 mol/L in acetone) and ultrasonicated for 15 min, followed by aging at 30 °C for 2 h. After filtration and drying at 50 °C for 12 h, the powders were calcined at 500 °C under a mixed N_2/O_2 atmosphere (85:15, v/v) for 60 min with a heating rate of 4 °C min^{-1}.

Preparation of amidoxime-functionalized polyethylene fibers

Ultra-high molecular weight polyethylene (UHMWPE) fibers were immersed in an emulsion of 5% glycidyl methacrylate (GMA) (2.5 mL GMA + 47.5 mL water + 0.25 g Tween-20). Nitrogen was bubbled through the emulsion for 15 min to remove oxygen. Fibers were irradiated with ^{60}Co γ-rays at 10 kGy with a dose rate of 1.67 kGy h^{-1}. After irradiation, fibers were Soxhlet-extracted with acetone for 24 h and dried at 60 °C. Then these fibers were immersed in 50% (v/v) of ethylene diamine solution in 1,4-dioxane at 80 °C for 3 h. Fibers were washed with ethanol and deionized water, then dried at 60 °C. Finally, the prepared fibers were immersed in a solution containing 0.5 mol/L hydroxylamine hydrochloride in a 1:1 water/dimethyl sulfoxide

(DMSO) mixture, and the pH was adjusted to 7 with Na_2CO_3. The GMA-modified fiber was reacted with this solution at 80 °C for 4 h. After the reaction, the fibers were washed with ethanol and deionized water, and then dried at 60 °C. The amidoxime functionalized fibers were thus obtained.

Fabrication of Fiber@HoMS

Square pieces of amidoxime-functionalized polyethylene fiber (each 10 mg) were first immersed in ethyl acetate and heated at 80 °C for 6 h to enhance surface accessibility. Subsequently, 0.16 mg of Ta_2O_5/C-HoMS powder was dispersed in 5 mL of ethyl acetate under ultrasonication. The pretreated fiber was then immersed in the dispersion and subjected to further ultrasonication to promote uniform coating. After deposition, the fiber was removed, rinsed thoroughly with ethyl acetate to remove loosely adhered particles, and dried under ambient conditions. The resulting Fiber@HoMS exhibited a visibly darkened surface. A pristine fiber piece of the same dimensions was kept unmodified as the control adsorbent.

Adsorption experiments

Batch adsorption experiments were conducted to evaluate the U(VI) uptake performance of the adsorbents under ambient pressure. In a typical procedure, 10 mg of adsorbent was immersed into a certain amount of uranyl nitrate solution within a customized beaker, as shown in the figures. The initial U(VI) concentration and solution pH were adjusted with trace amounts of 0.1 mol/L HCl or Na_2CO_3 as needed. To elucidate the role of the photo-thermal effect, comparative tests were performed: the Fiber@HoMS was exposed to simulated solar irradiation or kept under dark conditions as a control. All experiments were carried out in triplicate, and the reported adsorption data represent the mean values from three independent runs.

Uranium quantification via arsenazo III spectrophotometry

A standard curve for uranium quantification was established using the Arsenazo III chromogenic method. First, 500 mg/L Arsenazo III stock solution and 0.1 mol/L HCl solution were prepared. For each calibration point, 2 mL of the Arsenazo III solution and 0.5 mL of the HCl solution were added to a 10 mL volumetric flask, followed by the addition of a known volume of uranium standard solution to obtain final U(VI) concentrations of 0, 0.5, 1, 2, and 4 mg/L. After dilution to the mark and thorough mixing, the absorbance of each solution was measured at 651 nm using a UV-vis spectrophotometer. A linear calibration curve was plotted by correlating the absorbance with the corresponding uranium concentration (Figure S5). The formula for the standard curve is as follows: $A = 0.22062C + 0.06994$, where A represents absorbance, C represents solution concentration, with R^2 of 0.9999.

Photothermal adsorption testing

The photothermal uranium adsorption performance was evaluated using the Fiber@HoMS under simulated solar irradiation at an intensity of 1000 W/m^2, while all other experimental parameters remained consistent with the dark condition as a control (Figures S6). In a typical adsorption experiment, 10 mg of the adsorbent

was added to a certain amount (from 250 mL to 2.5 L) of uranium solution with an initial concentration (C_0) of 8 mg/L at room temperature (Figures S7 and S8). Samples were collected at predetermined time intervals to determine the residual uranium concentration (C_t). The adsorption capacity at time t, q_t (mg U/g adsorbent), was calculated using the following mass-balance equation:

$$q_t = (C_0 - C_t) \times V / m$$

where V is the volume of the solution (L) and m is the mass of the adsorbent (g). When adsorption reached equilibrium, the corresponding value was denoted as q_e, the equilibrium adsorption capacity.

Data availability

The original data are available from corresponding authors upon reasonable request.

Funding

This work was supported by the Project of Uranium Extraction from Seawater (HNKF202216 (36)), the National Natural Science Foundation of China (52572118, 92163209, 22293043), the Beijing Natural Science Foundation (JQ22004), and the Shenzhen University 2035 Program for Excellent Research (2024B005). D.W. thanks the financial support for Outstanding Scientific and Technological Innovation Talents Training Fund in Shenzhen.

Author contributions

S.S. performed the uranium extraction experiments, analyzed the data and drafted the manuscript. D.Y. synthesized the HoMS and conducted the inductively coupled plasma mass spectrometry (ICP-MS), optical absorption and photothermal measurements. S.Z. helped analyze the data and revise the manuscript. J.H. and G.W. fabricated the amidoxime-functionalized fibers. J.W. contributed to the scientific discussion. N.Y. and D.W. designed the experiments and revised the manuscript. D.W. conceived the project.

Conflict of interest

The authors declare no conflict of interest.

Supplementary information

The supporting information is available online at https://doi.org/10.1360/nso/20250084. The supporting materials are published as submitted, without typesetting or editing. The responsibility for scientific accuracy and content remains entirely with the authors.

References

1 Mirkhusanov UT, Semenova DY, Kharitonov VV. Forecasting the cost and volume of uranium mining for different world nuclear energy development scenarios. *Nucl Energy Technol* 2024; **10**: 131–137.
2 Shannak S', Cochrane L, Bobarykina D. Global uranium market dynamics: Analysis and future implications. *Int J Sustain Energy* 2025; **44**: 2457376.
3 Xie Y, Liu Z, Geng Y, *et al.* Uranium extraction from seawater: Material design, emerging technologies and marine engineering. *Chem Soc Rev* 2023; **52**: 97–162.
4 Degueldre C. Uranium as a renewable for nuclear energy. *Prog Nucl Energy* 2017; **94**: 174–186.
5 Peluzo TC, Kraka E. Uranium: The nuclear fuel cycle and beyond. *Int J Mol Sci* 2022; **23**: 4655.
6 Tsouris C. Uranium extraction: Fuel from seawater. *Nat Energy* 2017; **2**: 17022.
7 Wei G, Chen Z, Tai X, *et al.* Recent progress of uranium extraction and its catalytic applications. *Trans Tianjin Univ*

2025; **31**: 390–402.

8 Brook BW, Alonso A, Meneley DA, *et al.* Why nuclear energy is sustainable and has to be part of the energy mix. *Sustain Mater Technol* 2014; **1-2**: 8–16.

9 Zhang W, Wu M, Xin Y, *et al.* Comparative analysis of seawater uranium extraction materials: Toward the development of bio-based and biomimetic materials. *Coord Chem Rev* 2025; **534**: 216589.

10 Dungan K, Butler G, Livens FR, *et al.* Uranium from seawater—Infinite resource or improbable aspiration? *Prog Nucl Energy* 2017; **99**: 81–85.

11 Yuan Y, Cao D, Cui F, *et al.* High-capacity uranium extraction from seawater through constructing synergistic multiple dynamic bonds. *Nat Water* 2025; **3**: 89–98.

12 Zhang D, Liu L, Zhao B, *et al.* Highly efficient extraction of uranium from seawater by polyamide and amidoxime co-functionalized MXene. *Environ Pollution* 2023; **317**: 120826.

13 Sun Z, Chen Z, Tai X, *et al.* Uranium extraction from seawater: Methods and challenges. *Sci China Chem* 2025; **68**: 3923–3926.

14 Yuan Y, Yu Q, Cao M, *et al.* Selective extraction of uranium from seawater with biofouling-resistant polymeric peptide. *Nat Sustain* 2021; **4**: 708–714.

15 Wang T, Tao B, Zuo B, *et al.* Challenges and opportunities of uranium extraction from seawater: A systematic roadmap from laboratory to industry. *Small Methods* 2025; **9**: e2401598.

16 Yang Y, Lan F, Shi L, *et al.* Uranium extraction from seawater: Progress and challenges. *J Environ Chem Eng* 2026; **14**: 120945.

17 Yan G, Zuo B, Liu S, *et al.* Opportunities and challenges of capacitive deionization for uranium extraction from seawater. *Acta Physico-Chim Sin* 2025; **41**: 100032.

18 Song Y, Deng B, Wang K, *et al.* Highly-efficient adsorbent materials for uranium extraction from seawater. *J Environ Chem Eng* 2024; **12**: 113967.

19 Liu Z, Tan H, Shao Y, *et al.* Membrane-based adsorbent materials for uranium extraction from seawater: Recent progress and future prospects. *Nanoscale* 2025; **17**: 9764–9785.

20 Ding D, Zeng Q, He F, *et al.* The effect of thermal oxidation on the photothermal conversion property of tantalum coatings. *Materials* 2021; **14**: 4031.

21 Chen X, Yang N, Wang Y, *et al.* Highly efficient photothermal conversion and water transport during solar evaporation enabled by amorphous hollow multishelled nanocomposites. *Adv Mater* 2022; **34**: 2107400.

22 Mao D, Wang C, Li W, *et al.* Hollow multishelled structure: Synthesis chemistry and application. *Chem Res Chin Univ* 2024; **40**: 346–393.

23 Huang M, Lu K, Wang Z, *et al.* Thermally cross-linked amidoxime-functionalized polymers of intrinsic microporosity membranes for highly selective hydrogen separation. *ACS Sustain Chem Eng* 2021; **9**: 9426–9435.

24 Bai J, Ma X, Gong C, *et al.* A novel amidoxime functionalized porous resins for rapidly selective uranium uptake from solution. *J Mol Liquids* 2020; **320**: 114443.

25 Cui C, Wu J, Yu X, *et al.* New methodological research progress in uranium extraction from seawater. *Chem Res Chin Univ* 2025; **41**: 1557–1571.

26 Cui X, Ruan Q, Zhuo X, *et al.* Photothermal nanomaterials: A powerful light-to-heat converter. *Chem Rev* 2023; **123**: 6891–6952.

27 Zhang Y, Astrath NGC, Lukasievicz GVB, *et al.* Understanding and designing photothermal responses in complex layered systems. *Sci Rep* 2025; **15**: 26173.

28 Ramos-Fernandez EV, Rendon-Patiño A, Mateo D, *et al.* Photothermal catalysts, light and heat management: From materials design to performance evaluation. *Adv Energy Mater* 2025; **15**: 2405272.

29 Song YC, Ingram S, Arbon RE, *et al.* Transient cavity dynamics and divergence from the Stokes-Einstein equation in organic aerosol. *Chem Sci* 2020; **11**: 2999–3006.

30 Kerisit S, Liu C. Molecular simulation of the diffusion of uranyl carbonate species in aqueous solution. *Geochim*

Cosmochim Acta 2010; **74**: 4937–4952.

31 Murzin DY. From isotherms to modern kinetics. *Nat Catal* 2025; **8**: 861–862.

32 Shimizu S, Matubayasi N. Understanding sorption mechanisms directly from isotherms. *Langmuir* 2023; **39**: 6113–6125.

33 Zhang B, Gao B, Ma W, *et al.* Adsorption of uranium(VI) by natural vermiculite: Isotherms, kinetic, thermodynamic and mechanism studies. *J Environ Radioact* 2023; **270**: 107305.

34 Ezzati R, Azizi M, Ezzati S. A theoretical approach for evaluating the contributions of pseudo-first-order and pseudo-second-order kinetics models in the Langmuir rate equation. *Vacuum* 2024; **222**: 113018.

35 Aumeier BM, Augustin A, Thönes M, *et al.* Linking the effect of temperature on adsorption from aqueous solution with solute dissociation. *J Hazard Mater* 2022; **429**: 128291.

36 Estes SL, Powell BA. Enthalpy of uranium adsorption onto hematite. *Environ Sci Technol* 2020; **54**: 15004–15012.

37 Zhang M, Gao Q, Yang C, *et al.* Preparation of amidoxime-based nylon-66 fibers for removing uranium from low-concentration aqueous solutions and simulated nuclear industry effluents. *Ind Eng Chem Res* 2016; **55**: 10523–10532.

38 Yan M, Shao D. Management biofouling of uranium extraction from seawater by ultraviolet technique: Effect of UV wavelength. *Colloids Surfs A-Physicochem Eng Aspects* 2025; **704**: 135571.

39 Yan M, Gao Q, Shao D. Ultraviolet radiation restrains marine biofouling during uranium extraction from seawater. *Environ Sci-Water Res Technol* 2024; **10**: 3230–3237.

40 Gao Q, Hu J, Li R, *et al.* Radiation synthesis of a new amidoximated UHMWPE fibrous adsorbent with high adsorption selectivity for uranium over vanadium in simulated seawater. *Radiat Phys Chem* 2016; **122**: 1–8.